UNIVERSITÀ DI PARMA
ARCHIVIO DELLA RICERCA

University of Parma Research Repository

A Wi-Fi cloud-based portable potentiostat for electrochemical biosensors

This is the peer reviewd version of the followng article:

Original
A Wi-Fi cloud-based portable potentiostat for electrochemical biosensors / Bianchi, V., Boni, A., Fortunati, S., Giannetto, M., Careri, M., De Munari, I.. - In: IEEE TRANSACTIONS ON INSTRUMENTATION AND MEASUREMENT. - ISSN 0018-9456. - 69:6(2020), pp. 3232-3240. [10.1109/TIM.2019.2928533]

Availability:
This version is available at: 11381/2861364 since: 2024-10-03T09:06:39Z

Publisher:
Institute of Electrical and Electronics Engineers Inc.

Published
DOI:10.1109/TIM.2019.2928533

Terms of use:

Anyone can freely access the full text of works made available as "Open Access". Works made available

Publisher copyright

note finali coverpage

(Article begins on next page)

13 November 2026

This article has been accepted for publication in a future issue of this journal, but has not been fully edited. Content may change prior to final publication. Citation information: DOI 10.1109/TIM.2019.2928533, IEEE Transactions on Instrumentation and Measurement

A Wi-Fi cloud-based portable potentiostat for electrochemical biosensors

Valentina Bianchi, Andrea Boni, Simone Fortunati, Marco Giannetto, Maria Careri and Ilaria De Munari, *Member, IEEE*

***Abstract* — The measurement of the analyte concentration in electrochemical biosensors traditionally requires costly laboratory equipment to obtain accurate results. Innovative portable solutions have recently proposed, but usually they lean on PC or smartphones for data elaboration and they exhibit poor resolution or portability and proprietary software. This paper presents a low-cost portable system, assembling an ad-hoc designed analog front-end and a development board equipped with a system-on-chip integrating a microcontroller and a Wi-Fi network processor. The wireless module enables the transmission of measurements directly to a cloud service for sharing device outcome with users (physicians, caregivers, etc.). In doing so, the system does not require customized software nor other devices involved in data acquisition. Further, when any internet connection is lost, the data are stored on board for subsequent transmission when a Wi-Fi connection is available. The noise output voltage spectrum has been characterized. Since the designed device is intended to be battery-powered to enhance portability, investigations about battery lifetime were carried out. Finally, data acquired with a conventional benchtop Autolab PGSTAT-204 electrochemical workstation are compared with the outcome of our developed device to validate the effectiveness of our proposal. To this end, we selected ferri/ferrocyanide as redox probe, obtaining the calibration curves for both platforms. The final outcomes are shown to be feasible, accurate and repeatable.**

***Index Terms*—Portable potentiostat, Analog Front End, IoT, Wi-Fi, Cloud Services**

I. Introduction

The applications of Electrochemical Biosensors for identification of biologically active compounds have significantly increased over the past few years. The peculiarities of biosensors as enzyme-labelled immunosensors rely in time- and cost- effectiveness allowing to perform quantitative or semi-quantitative analyses not limited to simple qualitative screening usually associated to conventional immunochemical approaches such as Enzyme Linked Immunosorbent Assay (ELISA). Moreover, they represent a powerful diagnostic tool for domiciliary Point-of-Care Testing (POCT), based on reliable and inexpensive instrumentation that could be miniaturized in order to develop portable devices. In fact, the size of the equipment normally available limits portability, thus making it advisable to install it in dedicated and specifically equipped laboratories.

Recently, a lot of efforts have been dedicated to develop new electrochemical sensing devices and their associated electronics [1]–[3]. Among them, some portable solutions have been proposed [4]–[6]. These solutions were designed to be used in conjunction with a computer connected through a USB port or with a smartphone via Bluetooth (BT) for data elaboration. A portable potentiostat with wireless connectivity would facilitate electrochemical analysis at the point-of-use (on-site), where access to a computer or connection to a smartphone is difficult or uncomfortable. Moreover, this device should be low-cost and allowing for continued and large-scale monitoring.

In this paper, we present the prototype of a portable potentiostat suitable for the acquisition, processing and sharing of signal outputs from any kind of amperometric biosensor, ranging from label-free system based on reversible redox probes to enzyme sensors or enzyme-labelled immunosensors. In fact, all the above-cited systems are based on the acquisition of a signal output resulting from the application of a fixed or pulse-scanned potential input. The proposed device, equipped with a microcontroller integrating a Wi-Fi network processor, is connected to the Internet through a standard Wi-Fi router. The collected raw data are processed on board and the results are sent to a cloud environment for subsequent sharing with the user or stakeholders (e.g. physicians and caregivers), enabling remote monitoring features. In case of absence of any internet connection the raw data are stored on board for subsequent transmission when a Wi-Fi connection is available. This solution leans on a widespread protocol, commonly available at home and in most medical offices or clinics making the proposed device a flexible standalone solution. Moreover, the presented approach does not require the design of a dedicated software either for a Personal Computer (PC) or for a smartphone or other devices. Currently, cloud services allow sending messages (e.g. text messages, tweets, etc.). Such feature can be exploited to send the outcome of data elaboration directly on the smartphone or PC of the user/physician without the necessity of developing custom apps. This represents a relevant advantage with respect to other solutions presented in literature [7], [8] in terms of cost savings, reduced users'

Paper submitted for review on

V. Bianchi, A. Boni and I. De Munari are with the Department of Engineering and Architecture, University of Parma, 43124 Parma, Italy (e-mail: valentina.bianchi@unipr.it; andrea.boni@unipr.it; ilaria.demunari@unipr.it).

S. Fortunati, M. Giannetto and M. Careri are with the Department of Chemistry, Life Sciences and Environmental Sustainability, University of Parma, 43124 Parma, Italy (e-mail: simone.fortunati@studenti.unipr.it, marco.giannetto@unipr.it; maria.careri@unipr.it).

0018-9456 (c) 2019 IEEE. Personal use is permitted, but republication/redistribution requires IEEE permission. See http://www.ieee.org/publications_standards/publications/rights/index.html for more information.

This article has been accepted for publication in a future issue of this journal, but has not been fully edited. Content may change prior to final publication. Citation information: DOI 10.1109/TIM.2019.2928533, IEEE Transactions on Instrumentation and Measurement

burden, and mandatory technological skills .

The paper is organized in sections outlined below. In Section II, the state of the art in the field of portable potentiostat is presented, then, in Section III, the hardware of the prototypal device developed is described. In Section IV, the characterization measurements carried out are detailed and the device performance is evaluated. Concluding remarks are drawn in Section V.

II. Related Works

Most of the commercial-off-the-shelf portable potentiostats for potential-controlled current measurement techniques, such as voltammetric and galvanostatic [3], [9], [10], are based on the LMP91000 Analog Front-End (AFE) by Texas Instrument [11]. It acts as an interface between the sensor element and microcontroller, generating an output voltage proportional to the cell current. It is completely integrated into a single chip. It operates over a voltage range of 2.7 to 5.25 V with a current consumption of 10μA and a programmable current range from 2-to-250 μA, bipolar, (assuming an Analog to Digital Converter (ADC) with 1.4 V full-scale). This current range is acceptable for applications with medium to high analyte concentrations, but is not suitable for lower concentration ranges, leading to sub-microampere responses. In [7], [9] low-cost and miniaturized potentiostats for electrochemical immunosensing of cortisol are presented. In these works, the LMP9100 is interfaced with a microcontroller unit (MCU) for potentiostat settings and data reading and processing. Once data have been acquired, they are stored and elaborated into the internal memory of the MCU. Data are also sent to a PC through a Secured Shell communication to be elaborated and plotted with MATLAB. In these implementations to export processed data, a wired communication and a PC are always needed. In [12] a portable potentiostat based on similar hardware is presented. In this case, the authors add the possibility to communicate through Bluetooth protocols, enhancing the device portability. The MCU used in this application integrates an ADC with 12 bit of resolution, leading to a 0.8mV voltage resolution. The principal limitation of LMP9100 based applications, like the one presented in [13] is that this device allows to condition the electrochemical cell under test with a number of points considerably lower to that obtainable from bench-top instruments. For example, in [13] the analysis is done considering only 35 points in the conditioning voltage. This set-up is therefore perfect for qualitative, threshold-based applications whose purpose is to discriminate between disease-positive users and negative ones, but it is poor if a quantitative analysis is required. Thus, to carry out a precise measurement of the concentration it is advisable to build ad-hoc circuits that allow greater versatility.

Commercial instruments are also available in hand-held solutions from several companies. Examples are: PalmSens and EmStat (Palm Instruments) [4], PG581 (Uniscan Instruments) [14], 910 PSTAT mini (Metrohm) [15]. The commercial solutions are based on proprietary software and they require a USB or BT connection with smartphones or PC for data elaboration. Moreover, they are generally very expensive solutions.

Some portable potentiostats based on custom designed hardware have also been reported in literature [16]–[19].

In [16] a high precision low-cost potentiostat is described. High resolution is obtained exploiting a 20bit DAC and a 22bit ADC on board. Data sharing relies on an USB connection to a host PC.

In [17] a portable potentiostat based on a custom AFE is reported. The AFE is connected to a ATxmega32E5 MCU integrating a 12 bit DAC and a 12bit ADC. Once collected, data are sent through an UART connection to a PC where an R code processes and plots the data. In this solution, the output voltage resolution is 0.6mV, the current measurement range is ±100μA and the current noise (peak to peak) is 200nA.

In [18] a Bluetooth Arduino based potentiostat is described. It features a good resolution with a 3.3V power supply and 16-bits ADC and DAC. It needs a smartphone that processes the sample data and acts as a gateway between the potentiostat and a cloud service.

In general, all these solutions have a good resolution with respect to that obtainable with the LMP91000, and, in this, sense, they are comparable to traditional bench top instruments. However, they lack in portability: the use of some low range protocols or, in some cases, even the absence of wireless communication involves the need of another device to analyze and share the collected data. Using a long range, widespread wireless protocol such as Wi-Fi could overcome this problem [20].

In [19] a Wi-Fi portable potentiostat is presented In that system the AFE exploits a 12bit DAC, providing a nominal resolution of the reference voltage of 1.2mv. The opamp used in that design exhibits a relatively large input bias current (45 nA) and noise voltage (35 nV/$\sqrt{Hz}$). Moreover, the AFE exhibits a wireless connection (Wi-Fi), which allows data uploading to an open-source cloud-based server. Therefore, no PC or other tools are needed to perform analysis, similarly to the solution presented in [13]. Nevertheless, the portability of the potentiostat in [19] is compromised since a desktop power supply is required to provide with multiple supply levels (-8,-5,+5,+8 V) to the AFE.

III. Hardware Device

In this paper, a new compact Wi-Fi connected and battery-powered potentiostat is presented. The new device is intended for reading an immunosensor with a precision comparable to that of common laboratory equipment, but with decidedly smaller dimensions. This feature, combined with the possibility of processing data on board and transmitting it when a Wi-Fi connection becomes available, makes the device extremely portable and versatile and, at the same time, eliminates the need to exploit the connectivity of an additional device (laptop, smartphone etc.). The designed hardware consists of a custom designed AFE (Analog Front-End) and a microcontroller with an integrated Wi-Fi transceiver (CC3200 by Texas Instruments [21]).

0018-9456 (c) 2019 IEEE. Personal use is permitted, but republication/redistribution requires IEEE permission. See http://www.ieee.org/publications_standards/publications/rights/index.html for more information.

This article has been accepted for publication in a future issue of this journal, but has not been fully edited. Content may change prior to final publication. Citation information: DOI 10.1109/TIM.2019.2928533, IEEE Transactions on Instrumentation and Measurement

The AFE performs the conditioning of the cell and the measurement of the currents due to the chemical reaction, while the microcontroller unit (MCU) processes these currents by relating them to the applied voltages and transmits the data processed to a cloud service. In this prototype version we designed an AFE board to be connected with the CC3200 development platform. A more compact version of the device is planned, with both AFE and MCU embedded in the same board.

In Fig. 1 General System Architecturethe general system architecture is depicted.

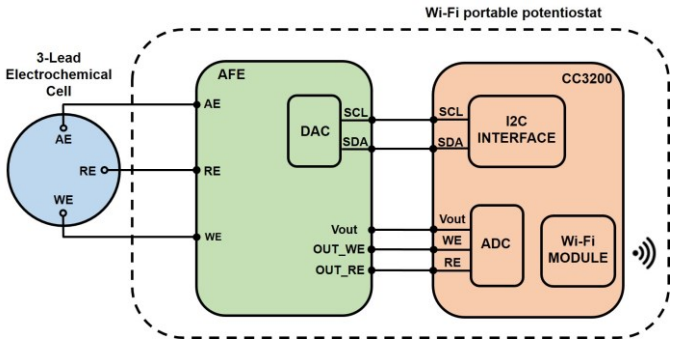

Fig. 1 General System Architecture

A. Amperometric sensors

The biosensors combined to the device presented in this paper belongs to the wide category of amperometric sensors. Typically, an amperometric sensor requires a three-electrodes elettrochemical cell consisting of a working electrode (WE), an auxiliary electrode (AE) and a reference electrode (RE). A classical method to measure the current output, related to the concentration of the target analyte, is the Differential Pulse Voltammetry (DPV) [22]. A known voltage bias is forced between WE and AE pins, V_{bias}, and the combination of faradic and capacitive sensor currents is measured. In Fig. 2 an example of conditioning V_{bias} is shown, where three fundamental parameters (the pulse interval time T_{PULSE}, the recovery interval time T_{REC}, and the step potential SP) are pointed out.

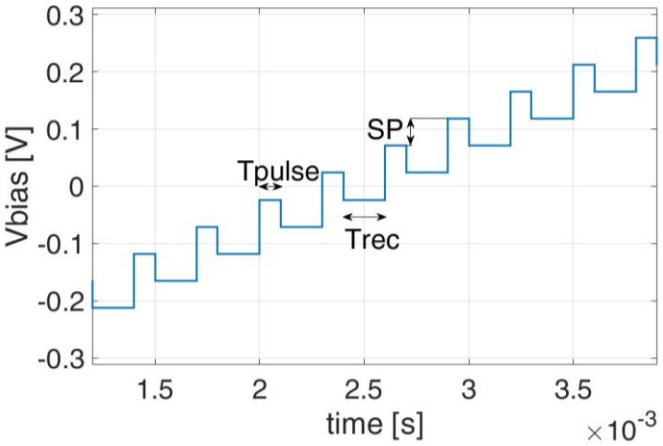

Fig. 2 Example of conditioning V_{Bias}

The current is measured at the beginning and at the end of each T_{PULSE}, and is processed in a differential mode. In this way the faradic component of the response (i.e. the analytical signal) is enhanced with respect to the capacitive current (i.e. the noise). The latter exponentially decreases over time, while faradic current decreases with the square root of the time. This differential signal exhibits a maximum whose intensity is related to the concentration of the target analyte. Other common techniques exploited to perform a concentration measurement with an electrochemical cell are the Chronoamperometry, used for example to assess the concentration of the dissolved Oxygen or glucose with enzymatic sensors [23], [24] and the Squared-Wave Voltammetry (SWV), which is the first choice for the determination of heavy metals at low concentrations [25]. Chronoamperometry is based on the application of fixed voltage and measurement of current vs time, whereas SWV requires a simple squared-wave signal with an amplitude comparable to that used for the DPV and a frequency in the 1-to-120Hz range. The amplitude of the generated currents is similar for the three techniques. In the rest of the paper reference will be made only to the DPV. However, it is worth to notice that the proposed potentiostat is not limited to the DPV, since the AFE circuit is fully compatible with the Chronoamperometry and the SWV signals and the signal processing section can properly manage all three techniques. In Fig. 3, the equivalent circuit of an amperometric cell is shown, where voltage source V_B models the voltage drop between AE and RE pins depending on the electrode process occurring in the cell.

In the following paragraph the reading circuitry is detailed.

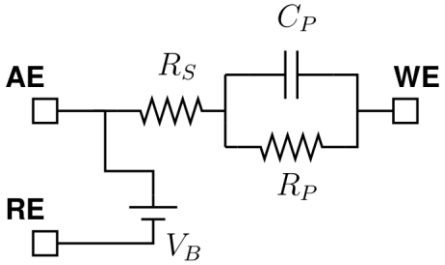

Fig. 3 Electric equivalent (lumped elements) of the amperometric cell

B. Analog Front-End

The schematic of the AFE circuit is shown in Fig. 4. The control amplifier *A1* provides the bias voltage to the cell, controlling the voltage at the AE electrode to keep the voltage at the RE pin almost equal to the programmable reference voltage V_{RA}. It is worth to notice that opamp A1 must exhibit an adequate output current capability in order to activate and maintain the chemical reaction in the cell. Another critical feature of the amplifier is the stability margin that must be carefully evaluated, considering the large capacitive load at the AE pin due to the cell (Fig. 3). A further critical specs of the control amplifier is the input-referred noise voltage which directly contributes to the potentiostat noise voltage measured between RE and WE pins. The control amplifier in the proposed design can deliver an output current as large as 30 mA, thus allowing a fast start-up of the reaction [26]. The simulated phase margin with the electric-equivalent of the sensor is about 80°. It is worth to notice that an LHP zero is found in the loop-gain due to the presence of the series resistance R_S in the sensor equivalent circuit (Fig. 3).

0018-9456 (c) 2019 IEEE. Personal use is permitted, but republication/redistribution requires IEEE permission. See http://www.ieee.org/publications_standards/publications/rights/index.html for more information.

This article has been accepted for publication in a future issue of this journal, but has not been fully edited. Content may change prior to final publication. Citation information: DOI 10.1109/TIM.2019.2928533, IEEE Transactions on Instrumentation and Measurement

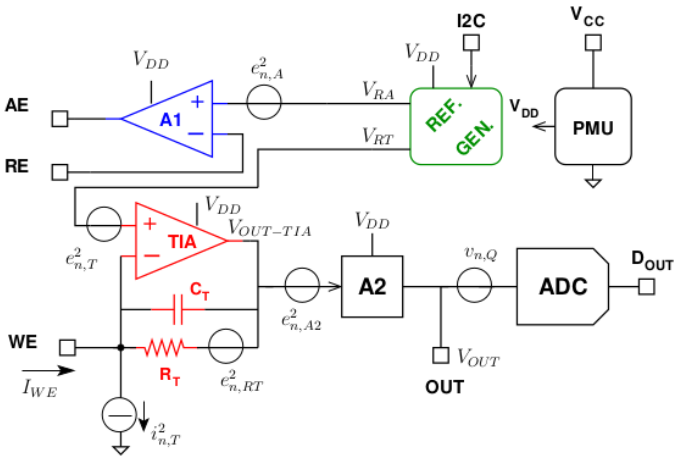

Fig. 4 Schematic circuit of the Analog Front-End with noise sources.

The transimpedance amplifier (TIA) in Fig. 4 implements the required signal conditioning of the cell current at the WE terminal. The TIA gain can be varied from 10 to 100 V/mA by means of the programmable feedback resistance R_T. The capacitor C_T allows to achieve an adequate stability margin [27],[28].

The voltage output range and offset are set through the feedback resistor (range) and the reference voltage V_{RT} (output offset). Since the input voltage of the A/D converter (ADC) embedded in the MCU must be limited to 1.8 V (ratings) [21], an attenuator is introduced, A2, for limiting the output voltage (V_{OUT}) to a safe level even in the case of saturation occurring in the TIA (i.e. $V_{OUT-TIA}$ equal to the AFE supply). Such attenuator exhibits a first-order transfer function, $H_{A2}(f)$, with equivalent noise bandwidth $N_{BW,A2}$ equal to approximately 110 Hz.

The programmable reference voltages for the control (V_{RA}) and the transimpedance (V_{RT}) amplifiers are generated by means of a dual D/A converter (DAC) with I2C digital inputs [27]. The power management unit provides the 3.3 V regulated supply voltage to the AFE circuits from the 5 V supply of the MCU. In the case of a cell which requires a higher voltage bias, the PMU can be programmed to provide the 5 V supply of the MCU to the AFE.

Furthermore, the AFE system allows to detect the voltage at RE and WE pins. This is mandatory in order to assess the position of the current peak with respect to the V_{bias}. This position is referable to the nature of the electroactive species under test. The sensing circuit for the WE voltage is shown in Fig. 5. It is worth to notice that the negative input pin of the TIA opamp is a critical net since any additional capacitance reduces the stability margin. Furthermore, the input current of the voltage sensing circuit adds to the sensor output current, I_{WE}. For this reason, an opamp featuring an input current in the pA range was used in the unity-gain configuration as the first stage of the WE sensing circuit [28]. The low-pass resistive attenuator (R1,R2,C1) is mandatory to limit the output voltage below the rated maximum input voltage of the A/D converter in the MCU and to limit the output noise.

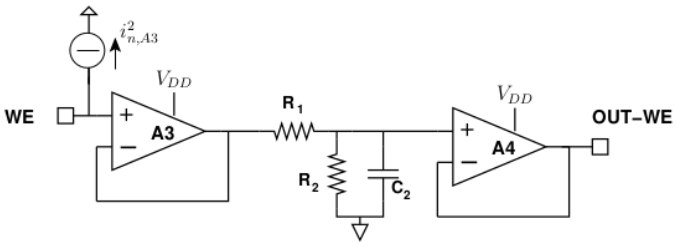

Fig. 5 Circuit schematic for sensing voltage at the WE pin.

C. Noise Analysis

The resolution of the concentration measurement is defined by the AFE circuit and the amperometric sensor. Limiting the analysis to the AFE, the effect of the thermal and supply noise sources at the ADC input are evaluated. With reference to Fig. 4, the amplifier A1 injects a current noise at the input of the transimpedance amplifier through the equivalent impedance of the sensor between AE and WE terminals, Z_C:

$$i^2_{n,WE,A} = \frac{e^2_{n,A}}{|Z_C|^2} \qquad (1)$$

where the input noise current of A1 was neglected and $e^2_{n,A}$ is the Power Spectral Density (PSD) of the overall noise voltage at its input. Such noise includes the input-equivalent noise voltage of the opamp (A1), its input-equivalent supply noise, and the additive noise affecting the reference voltage V_{RA}. The last term is caused by the DAC generating the programmable reference voltages in the AFE. The effect of the supply noise is estimated by the power supply rejection ratio (PSRR) of the opamp [29]. The equivalent impedance of the sensor is obtained by the equivalent lumped circuit of Fig. 3:

$$Z_C(f) \cong R_P \frac{1 + j\,2\,\pi\,C_P\,R_S\,f}{1 + j\,2\,\pi\,C_P\,R_P\,f} \qquad (2)$$

where $R_S \ll R_P$ was considered in the approximated expression. Therefore, the PSD of the noise voltage at the ADC input due to A1 is:

$$e^2_{n,OUT,A} = i^2_{n,WE,A} \cdot |Z_T|^2 \cdot |H_{A2}(f)|^2 \qquad (3)$$

where Z_T is the feedback impedance.

The contribution of the transconductance amplifier to the output noise voltage is due to the input-equivalent noise current of the TIA opamp, $i^2_{n,T}$, and of amplifier A3 in Fig. 5, $i^2_{n,A3}$, together with the involved noise voltage sources. The last contribution includes the thermal noise of the feedback resistor, $e^2_{n,RT}$, together with the combination of the input-equivalent noise voltage of TIA opamp (including the supply noise effect) and of the additive noise of reference V_{RT}, $e^2_{n,T}$. Therefore, the expression of the TIA contribution to the noise at the ADC input is obtained by circuit analysis:

$$e^2_{n,OUT,T} = \left[\left(i^2_{n,T} + i^2_{n,A3}\right) \cdot |Z_T|^2 + e^2_{n,RT} + e^2_{n,T} \cdot \left|1 + \frac{Z_T}{Z_C}\right|^2\right] \cdot |H_{A2}(f)|^2 \qquad (4)$$

where usually $|Z_C| \gg |Z_T|$ at low frequency. The overall PSD

0018-9456 (c) 2019 IEEE. Personal use is permitted, but republication/redistribution requires IEEE permission. See http://www.ieee.org/publications_standards/publications/rights/index.html for more information.

This article has been accepted for publication in a future issue of this journal, but has not been fully edited. Content may change prior to final publication. Citation information: DOI 10.1109/TIM.2019.2928533, IEEE Transactions on Instrumentation and Measurement

of the noise voltage at the ADC input includes the contributions of the attenuator block, $e_{n,A2}^2$:

$$e_{n,OUT}^2 = e_{n,OUT,A}^2 + e_{n,OUT,T}^2 + e_{n,A2}^2 \cdot |H_{A2}(f)|^2 \quad (5)$$

The Signal-to-Noise and quantization ratio at the AFE output is therefore:

$$SNQR_{OUT} = \int_{f_L}^{\infty} e_{n,OUT}^2 \, df + \frac{V_{OUT,pp}}{\sqrt{8} \cdot v_{n,Q}^2} \quad (6)$$

where $v_{n,Q}^2$ is the quantization noise voltage [30] and $V_{OUT,pp}$ is the peak-to-peak value of the voltage signal at AFE output. In the proposed potentiostat the ADC exhibit 12-b nominal resolution over a 1.4 V conversion range, leading to a quantization noise of about 100 μV_{rms}. Since the current output is obtained by the difference of the signals sampled at the beginning and at the end of each T_{PULSE}, the lower bound for noise integration, f_L, corresponds to the inverse of T_{PULSE}, which, for an optimal signal-to-noise ratio (faradic versus capacitive) is in the range of 100 ms [31].

The upper bound of the peak-to-peak value of the output signal depends on the lower output saturation of the TIA opamp (i.e. about 0 V in the present design) and on the ADC conversion range. The ADC embedded in the MCU exhibits an unipolar conversion range from 0 V to V_{FS}, i.e. 1.4 V [21].

Therefore, the output signal swing is maximized if the following conditions are fulfilled:

$$V_{RT}^* \cong \frac{V_{FS}}{2 \cdot H_{A2}(0)} \quad (7)$$

$$R_T^* = \frac{V_{RT}}{|I_{WE}|_{MAX}} \quad (8)$$

where $|I_{WE}|_{MAX}$ is the expected maximum of the absolute value of the input current and the frequency of the input signal is assumed to be well below the 3-dB frequency of TIA and A2 blocks. It is worth to notice that the value of V_{RT} allowing the maximum output swing, i.e. V_{RT}^*, may not lead to the maximum achievable value of the voltage bias (absolute value) between the RE and the WE pins, V_{bias}, which is, indeed, limited by the AFE supply voltage, V_{DD}:

$$|V_{bias}| \leq Min[V_{RT}, 2 \cdot (V_{DD} - V_{RT})] \quad (9)$$

The $SQNR_{OUT}$, of the potentiostat is maximized if the signal amplitude is maximized as well, provided that the impact of the thermal noise of the feedback resistor R_T is negligible with respect to the other noise sources.

D. Signal processing board

The processing core of the designed system is the system-on-chip (SoC) CC3200 by Texas Instruments. This SoC exploits an ARM Cortex-M4 MCU and a transceiver compliant with the IEEE 802.11b/g/n network protocol radio. For prototyping purposes, the CC3200 development board [32] was exploited in this study.

The MCU takes care of controlling the AFE DAC for the suitable conditioning of the amperometric sensor. To set-up the DAC registers an I2C communication port is exploited. Moreover, the WE, RE and Vout pins from the AFE board were connected to the 12bit ADC embedded in the CC3200 to acquire signals for subsequent elaboration. The processed data are then sent to a cloud service for remote consultation through the Wi-Fi interface. The sensor can be connected to different cloud environments coding conveniently the access method into the device firmware. In the present work an IoT open platform Thinkspeak© was adopted, but any other cloud platform (e.g. IBM bluemix, Microsoft Azure etc), can be exploited as well.

To allow the measurement of the analyte even if the connection is absent, and to limit the power consumption due to the Wi-Fi transmission, the acquired data are processed on board to extract meaningful information.

E. Conditioning and elaboration

Once V_{bias}, is applied to the amperometric cell, V_{WE}, V_{RE} and V_{out} are acquired, being respectively the voltage at WE, RE pins and the AFE output voltage (Fig. 1).

Then, data are multiplied by a constant, K, for taking into account the effect of the attenuator placed between the TIA and the the ADC input. For each measurement point, a current value is calculated following the equation:

$$I = \frac{V_{out} - V_{WE}}{G} \quad (10)$$

where G is the programmable gain of the TIA. As stated above, for a conventional DPV measurement the analyte concentration is related to the value of the peak from the differential current sampled at the beginning and at the end of each pulse. Considering a voltage range spanning from -0.4V and +0.4V, suitable for the ferri/ferrocyanide redox probe, and a step potential (SP) of 5mV a total of 302 measurement points were considered here compared to only 35 points of the LMP91000 based version [13]. This leads to 151 measurement points for each acquisition. This number is fully compatible with that of the most common bench instruments.

In order to properly estimate the value of the current peak a further processing has to be introduced. As the baseline of the differential current is frequently not perfectly parallel to the x-axis (baseline drift), it is not possible to apply simple methods for searching the maximum to evaluate the amplitude of the peak in the obtained current waveform. For this purpose, before peak evaluation, a baseline search and calculation algorithm was introduced for each measurement. Thirty absolute minimum points were identified for each waveform and a baseline was estimated using a linear polynomial fitting. This baseline is then used as a reference to calculate the actual peak amplitude, as shown in Fig. 6.

0018-9456 (c) 2019 IEEE. Personal use is permitted, but republication/redistribution requires IEEE permission. See http://www.ieee.org/publications_standards/publications/rights/index.html for more information.

This article has been accepted for publication in a future issue of this journal, but has not been fully edited. Content may change prior to final publication. Citation information: DOI 10.1109/TIM.2019.2928533, IEEE Transactions on Instrumentation and Measurement

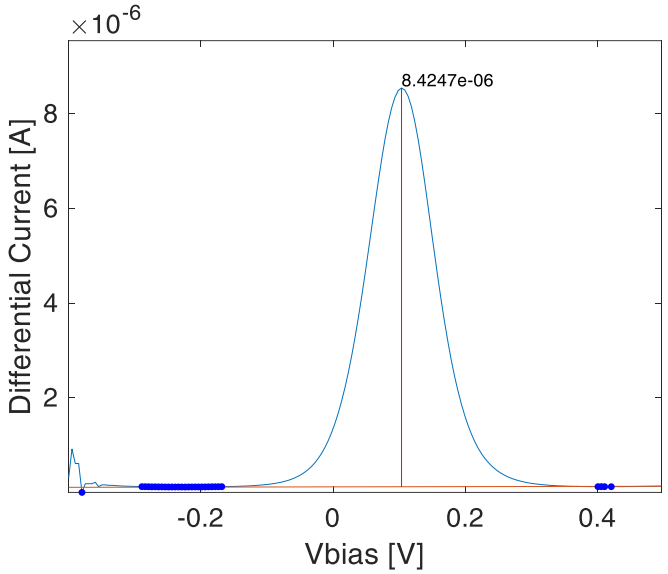

Fig. 6 Example of current peak value measurement with baseline assessment.

Finally, the computed peak value can either be sent to a cloud service for subsequent remote monitoring or can be stored in the device waiting for an available Wi-Fi connection.

IV. EXPERIMENTAL RESULTS

Tab. I reports a specs comparison of an integrated potentiostat AFE [11], a couple of systems with wireless connectivity, i.e. [4] and [19], and the proposed device. In the same Table, $V_{bias,n}$ is the voltage noise between WE and RE pins, over the 0.1-10 Hz bandwidth, $e_{n\text{-}RE}$ and $I_{B\text{-}RE}$ are the PSD noise voltage and the input bias current at the RE pin, NL_{TIA} is the measured TIA non linearity, $I_{WE\text{-}RES}$ is the nominal resolution of the current measurement, and $V_{RA\text{-}RES}$ is the minimum programmable step of the V_{RA} reference, Fig. 4. The comparison highlights the excellent performance in terms of noise, input current and resolution of the amplifier input voltage. Furthermore, the proposed potentiostat requires a single supply

TABLE I
SPEC.S COMPARISON

Spec	[19]	[11]	[4]	*Proposed*	*Unit*
$V_{bias,n}$	*N.A.*	*5.2*	*N.A.*	*3.1*	μV_{pp}
Max[I_{OUT}]	*8*	*10*	*20*	*30*	*mA*
$I_{B\text{-}RE}$	$4.8{\cdot}10^3$	*90*	*N.A.*	*1*	*pA*
$e_{n\text{-}RE}$ @ *10 kHz*	*35*	*N.A.*	*N.A.*	*6.5*	$nV/\sqrt{Hz}$
NL_{TIA}	*N.A.*	*5*	*N.A.*	*0.3*	*%*
$I_{WE\text{-}RES}$	*0.015*	*N.A.*	*1*	*0.25*	*‰*
$V_{RA\text{-}RES}$	$1.2{\cdot}10^3$	$66{\cdot}10^3$	*100*	*50*	*μV*
Supply	*-8,-5,+5,+8*	*2.7/5.5*	*+3,-3*	*3.3/5.5*	*V*
Connectivity	*WiFi*	*No*	*BT*	*WiFi*	

For [19] $I_{B\text{-}RE}$ and $e_{n\text{-}RE}$ are obtained from opamp datasheet and simulation model.

(either from a battery or a USB source), unlike the systems in [4] and [19].

The measured spectrum of the noise voltage at the output pin in Fig. 4Fig. 4, OUT, is shown in Fig. 7 together with the simulation results. The circuit model of the opamps in the proposed design includes both the input-equivalent voltage and current noise. The output noise of the DAC was added to the simulation test bench by means of a noisy resistor in series to each V_{RT} and V_{RA} voltage source, since a simulation model of such device was not available. The value of such resistor was defined on the basis of the PSD reported in the data-sheet at a few frequency points [27]. The noise measurement was carried out with a SR785 FFT analyzer, featuring a noise floor of about $10\ nV/\sqrt{Hz}$, and with a dummy cell, Fig. 3, connected to the AFE. It is worth to notice that the measured noise is slightly lower than the simulation results, even though the effect of the supply noise was non taken into account in the noise simulation. The frequency shaping of both simulation and measurement data are in excellent agreement.

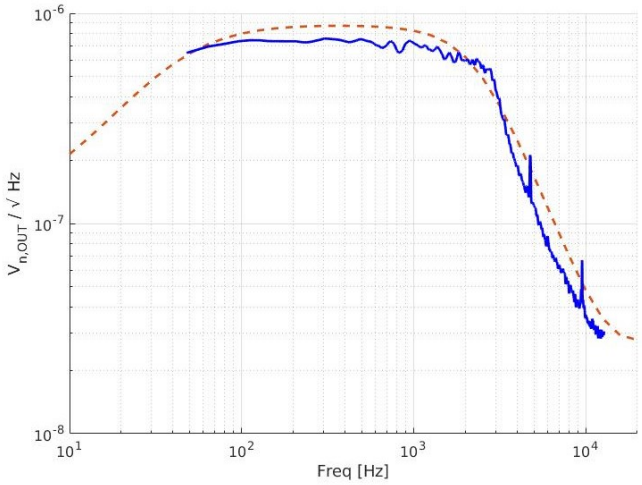

Fig. 7 Noise spectrum of the output voltage, V_{OUT}. Dashed line: simulation results; solid line: measured noise.

To validate the system, we carried out differential measurements with the proposed system, using different concentration levels of ferri/ferrocyanide redox probe in aqueous 100 mM KCl as supporting electrolyte. Measurements were performed on disposable Screen-Printed Electrodes from Dropsens (Metrohm) with glassy carbon WE and AE and silver RE. The electrochemical cell consists of 50 μL of redox probe solution casted on the three-electrode Screen-Printed chip. A preconditioning potential of -0.4 V was applied for 30 s in order to preconcentrate the ferrocyanide prior to its oxidation to ferricyanide. The findings were compared with analogous measurements performed using the conventional benchtop instrument (Autolab PGSTAT-204 electrochemical workstation, by Metrohm [33]). For this purpose, five different concentrations of redox probe were investigated, namely 100, 125, 250, 350 and 500 μM: for each concentration a 50% of ferricyanide and 50% ferrocyanide have been used. Three replicates were acquired for each concentration level.

In Fig. 8 the differential currents measured as a function of the bias voltage using the proposed system are shown. For the

0018-9456 (c) 2019 IEEE. Personal use is permitted, but republication/redistribution requires IEEE permission. See http://www.ieee.org/publications_standards/publications/rights/index.html for more information.

This article has been accepted for publication in a future issue of this journal, but has not been fully edited. Content may change prior to final publication. Citation information: DOI 10.1109/TIM.2019.2928533, IEEE Transactions on Instrumentation and Measurement

sake of clarity, for each concentration the average of the three replicates are reported.

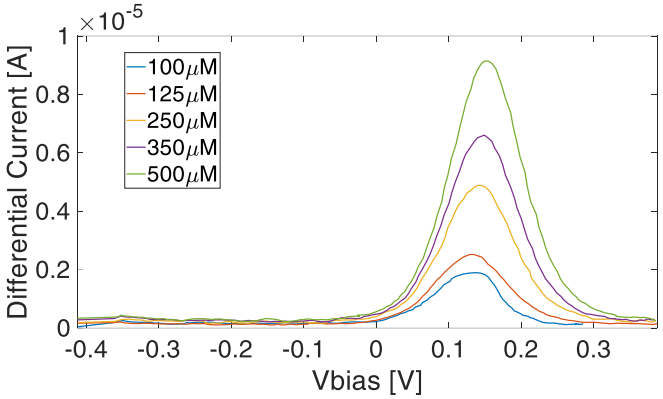

Fig. 8 Measured bias signal and current using the proposed system

In Fig. 9 a comparison between the data acquired with the new portable potentiostat and the AUTOLAB is shown.

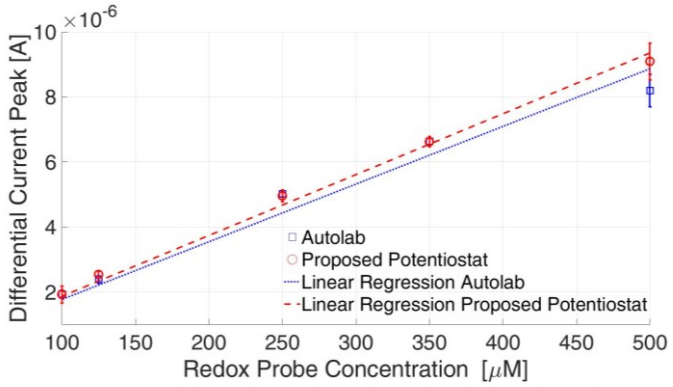

Fig. 9 Comparison of the calibration lines obtained with the redox probe using the proposed potentiostat and the Autolab benchtop instrument. The center and the length of the error bars correspond to the measured average and standard deviation at each concentration on three replicates.

The current outputs from both instruments evidenced high repeatability with relative standard deviation <10% for all the explored concentrations. In addition, the responses measured at the same concentration on the two instruments are almost superimposable. The linear interpolation of both datasets evidenced intercepts not significantly different *($p>0.05$)* from zero, whereas the slope values ($1{,}87\pm0{,}03\cdot10^{-8}$ for the proposed device and $1{,}77\pm0{,}04\cdot10^{-8}$ for the benchtop instrument) resulted to be not significantly different (*$p>0.01$*).

An assessment of the battery lifetime was carried out, considering a typical situation of one user and five acquisitions carried out per day. When the sensor is not measuring, it is forced into HIBERNATE mode. The power consumption of the CC3200 in different sleep modes has already been analyzed in [34]. The preconditioning time was set at 30s, T_{PULSE} at 100ms, T_{REC} at 200ms and 302 points for each measurement were considered. These were found as best conditions in terms of signal-to-noise ratio, sensitivity and repeatability of the output, to be used for quantitative analyses. The current drained by the sensor was measured using a LeCroy HDO6034 oscilloscope connected to a LeCroy AP015 current probe. In Table II measured currents and times are reported.

TABLE II
CURRENT CONSUMPTION OF THE PROPOSED POTENTIOSTAT

Interval Time	*Current[A]*	*Time[s]*
Preconditioning	*37.7e-3*	*30*
T_{PULSE}	*43e-3*	*100e-6*
T_{REC}	*38e-3*	*200e-6*
Data Transmission	*64.3e-3*	*2.96*
HIBERNATE	*5.2e-6*	*[]*

The average current drained during one day in these conditions was found to be 81μA. This leads to an estimated battery lifetime of 3.8 years, considering two 1.5V, 2700mAh standard AA batteries.

V. CONCLUSION

In this paper a new low-cost portable Wi-Fi potentiostat was presented. This device is based on a custom AFE board designed to maximize the measurement resolution while containing costs, to allow precise quantitative analyte concentration assessment, unlike a threshold based approach [13].

The presented system relies also on the CC3200 Wi-Fi MCU by Texas Instruments; it takes care of data sampling, processing and transmitting electrochemical data to a cloud service. In this realization, the open-source cloud service Thinkspeak was considered but, using a standard protocol, other cloud services are possible too. Exploiting cloud services allows the measurement result to be examined both by the user but also by other potential professionals (e.g. medical doctors) allowing for remote monitoring. A wireless communication and the possibility of a power supply of 3.3V enhance the portability, allowing the system to be battery powered. Battery lifetime was estimated resulting in 3.8 years.

The proposed potentiostat was also accurately characterized. The transimpedance amplifier in the AFE exhibits a non-linearity lower than 0.5%. The measured noise at the ADC input is in good agreement with the simulation results. Considering the ADC resolution and AFE noise an overall resolution of 0.025% is achieved in the voltage measurement.

Finally, measurements carried out with Autolab PGSTAT-204 electrochemical workstation are compared with the outcome of our device to validate the effectiveness of our proposal. The comparison highlights a good performance, fully suitable for amperometric biosensors for qualitative and quantitative purposes.

ACKNOWLEDGMENT

The authors would like to thank Mirco Mongilli, Enrico Panciroli and Marco Zagatti for their contribution in the design and test of the device presented in this work.

REFERENCES

[1] S. Ghanbari, M. Habibi, and S. Magierowski, "A High-Efficiency Discrete Current Mode Output Stage Potentiostat Instrumentation

0018-9456 (c) 2019 IEEE. Personal use is permitted, but republication/redistribution requires IEEE permission. See http://www.ieee.org/publications_standards/publications/rights/index.html for more information.

This article has been accepted for publication in a future issue of this journal, but has not been fully edited. Content may change prior to final publication. Citation information: DOI 10.1109/TIM.2019.2928533, IEEE Transactions on Instrumentation and Measurement

for Self-Powered Electrochemical Devices," *IEEE Trans. Instrum. Meas.*, vol. 67, no. 9, pp. 2247–2255, Sep. 2018.

[2] T. R. Molderez, X. Zhang, K. Rabaey, and M. Verhelst, "A Current-Driven Six-Channel Potentiostat for Rapid Performance Characterization of Microbial Electrolysis Cells," *IEEE Trans. Instrum. Meas.*, pp. 1–9, 2019.

[3] A. M. Pernia, M. J. Prieto, I. C. Orille, J. A. Martin-Ramos, and A. Costa-Garcia, "Development of Optimized Screen-Printed Immunosensors," *IEEE Trans. Instrum. Meas.*, vol. 58, no. 7, pp. 2181–2188, Jul. 2009.

[4] "Palmsens." [Online]. Available: https://www.palmsens.com/product/emstat-blue/. [Accessed: 07-Mar-2019].

[5] S. Chhorn and A. Teeramongkonrasmee, "A Portable USB-controlled Potentiostat for Paper-based Electrochemical Applications," in *2018 15th International Conference on Electrical Engineering/Electronics, Computer, Telecommunications and Information Technology (ECTI-CON)*, 2018, pp. 321–324.

[6] A. A. Rowe *et al.*, "CheapStat: An Open-Source, 'Do-It-Yourself' Potentiostat for Analytical and Educational Applications," *PLoS One*, vol. 6, no. 9, p. e23783, Sep. 2011.

[7] P. Bezuidenhout, S. Smith, K. Land, and T.-H. Joubert, "A low-cost potentiostat for point-of-need diagnostics," in *2017 IEEE AFRICON*, 2017, pp. 83–87.

[8] J. Kim *et al.*, "Wearable salivary uric acid mouthguard biosensor with integrated wireless electronics," *Biosens. Bioelectron.*, vol. 74, pp. 1061–1068, Dec. 2015.

[9] A. F. D. Cruz, N. Norena, A. Kaushik, and S. Bhansali, "A low-cost miniaturized potentiostat for point-of-care diagnosis," *Biosens. Bioelectron.*, vol. 62, pp. 249–254, Dec. 2014.

[10] J. Aznar-Poveda *et al.*, "A COTS-Based Portable System to Conduct Accurate Substance Concentration Measurements," *Sensors*, vol. 18, no. 2, p. 539, Feb. 2018.

[11] "LMP91000 Configurable AFE Potentiostat for Low-Power Chemical Sensing Applications | TI.com." [Online]. Available: http://www.ti.com/product/LMP91000. [Accessed: 08-Mar-2019].

[12] V. Raj, S. Ab, J. Stanley, and T. G. Satheeshbabu, "Fabrication of a Configurable Multi-Potentiostat for LOC Applications," 2018.

[13] M. Giannetto, V. Bianchi, S. Gentili, S. Fortunati, I. De Munari, and M. Careri, "An integrated IoT-Wi-Fi board for remote data acquisition and sharing from innovative immunosensors. Case of study: Diagnosis of celiac disease," *Sensors Actuators B Chem.*, vol. 273, pp. 1395–1403, Nov. 2018.

[14] "PG581." [Online]. Available: https://www.bio-logic.net/products/potentiostat-galvanostat-eis/pg581-portable-potentiostatgalvanostat/. [Accessed: 05-Apr-2019].

[15] "PSTAT910." [Online]. Available: https://www.metrohm-autolab.com/Products/Echem/PortablePot/PSTAT910.html. [Accessed: 05-Apr-2019].

[16] T. Dobbelaere, P. M. Vereecken, and C. Detavernier, "A USB-controlled potentiostat/galvanostat for thin-film battery characterization," *HardwareX*, vol. 2, pp. 34–49, Oct. 2017.

[17] S. Adams, E. H. Doeven, K. Quayle, and A. Kouzani, "MiniStat: Development and evaluation of a mini-potentiostat for electrochemical measurements," *IEEE Access*, pp. 1–1, 2019.

[18] A. Ainla *et al.*, "Open-Source Potentiostat for Wireless Electrochemical Detection with Smartphones," *Anal. Chem.*, vol. 90, no. 10, pp. 6240–6246, May 2018.

[19] C. Mercer, R. Bennett, P. Ó. Conghaile, J. F. Rusling, and D. Leech, "Glucose biosensor based on open-source wireless microfluidic potentiostat," *Sensors Actuators B Chem.*, Feb. 2019.

[20] M. Bassoli, V. Bianchi, and I. De Munari, "A plug and play IoT Wi-Fi smart home system for human monitoring," *Electron.*, vol. 7, no. 9, 2018.

[21] "CC3200 wireless MCU." [Online]. Available: http://www.ti.com/product/CC3200. [Accessed: 19-Mar-2019].

[22] D. Krulic, N. Fatouros, and M. . El Belamachi, "Stepped-potential voltammetries at stationary electrodes Part 1. Differential staircase, differential pulse and square-wave voltammetries," *J. Electroanal. Chem.*, vol. 385, no. 1, pp. 33–38, Mar. 1995.

[23] L. Hutton, M. E. Newton, P. R. Unwin, and J. V. Macpherson, "Amperometric Oxygen Sensor Based on a Platinum Nanoparticle-Modified Polycrystalline Boron Doped Diamond Disk Electrode," *Anal. Chem.*, vol. 81, no. 3, pp. 1023–1032, 2009.

[24] H. Lee, Y. J. Hong, S. Baik, H. Taeghwan, and D. Kim, "Enzyme-Based Glucose Sensor: From Invasive to Wearable Device," *Adv. Healthc. Mater.*, vol. 7, p. 1701150, 2018.

[25] M. Valentin, R. Gulaboski, M. Lovric, I. Bogeski, R. Kappl, and M. Hoth, "Square-Wave Voltammetry: A Review on the Recent Progress," *Electroanalysis*, vol. 25, pp. 2411–2422259, 2013.

[26] "AD8605-Precision, Low Noise, CMOS, RRIO Op Amp (single) | Analog Devices." [Online]. Available: https://www.analog.com/en/products/ad8605.html. [Accessed: 08-Mar-2019].

[27] "AD5667-Dual, 16-Bit nanoDAC® with I2C® Interface | Analog Devices." [Online]. Available: https://www.analog.com/en/products/ad5667.html. [Accessed: 08-Mar-2019].

[28] "OPA4170-36V, microPower, Rail-to-Rail Output, Quad, General Purpose Op Amp | Texas Instruments." [Online]. Available: http://www.ti.com/product/OPA4170. [Accessed: 08-Mar-2019].

[29] M. S. J. Steyaert and W. M. C. Sansen, "Power supply rejection ratio in operational transconductance amplifiers," *IEEE Trans. Circuits Syst.*, vol. 37, no. 9, pp. 1077–1084, 1990.

[30] B. Widrow, "Statistical analysis of amplitude-quantized sampled-data systems," *Trans. Am. Inst. Electr. Eng. Part II Appl. Ind.*, vol. 79, no. 6, pp. 555–568, 1961.

[31] A. Bello, M. Giannetto, G. Mori, R. Seeber, F. Terzi, and C. Zanardi, "Optimization of the DPV potential waveform for determination of ascorbic acid on PEDOT-modified electrodes," *Sensors Actuators B Chem.*, vol. 121, no. 2, pp. 430–435, Feb. 2007.

[32] "CC3200 Launchpad." [Online]. Available: http://www.ti.com/tool/CC3200-LAUNCHXL. [Accessed: 08-Apr-2019].

[33] "uAutolab." [Online]. Available: https://www.ecochemie.nl/Products/Echem/CompactNonModular/uAUTIII.html. [Accessed: 10-Apr-2019].

[34] M. Bassoli, V. Bianchi, I. De Munari, and P. Ciampolini, "An IoT Approach for an AAL Wi-Fi-Based Monitoring System," *IEEE Trans. Instrum. Meas.*, 2017.

0018-9456 (c) 2019 IEEE. Personal use is permitted, but republication/redistribution requires IEEE permission. See http://www.ieee.org/publications_standards/publications/rights/index.html for more information.